CHIN. PHYS. LETT. Vol. 37, No. 12 (2020) 127301

Fano Effect and Spin-Polarized Transport in a Triple-Quantum-Dot Interferometer Attached to Two Ferromagnetic Leads

Jiyuan Bai(白继元)[1], Kongfa Chen(陈孔发)[2*], Pengyu Ren(任鹏宇)[1], Jianghua Li(李江华)[1], Zelong He(贺泽龙)[1*], and Li Li(李立)[3]

[1]*School of Electronic and Information Engineering, Yangtze Normal University, Chongqing 408003, China*
[2]*College of Materials Science and Engineering, Fuzhou University, Fuzhou 350108, China*
[3]*Key Lab of In-fiber Integrated Optics of Ministry of Education, College of Science, Harbin Engineering University, Harbin 150001, China*

(Received 7 August 2020; accepted 15 October 2020; published online 8 December 2020)

We report the conductance and average current through a triple-quantum-dot interferometer coupled with two ferromagnetic leads using the nonequilibrium Green's function. The results show that the interference between the resonant process and the non-resonant process leads to the formation of Fano resonance. More Fano resonances can be observed by applying a time-dependent external field. As a Zeeman magnetic field is applied, the spin-up electron transport is depressed in a certain range of electron energy levels. A spin-polarized pulse device can be realized by adjusting the spin polarization parameters of ferromagnetic leads. Moreover, the I–V characteristic curves show that under the influence of Fano resonance, the spin polarization is significantly enhanced by applying a relatively large reverse bias voltage. These results strongly suggest that the spin-polarized pulse device can be potentially applied as a spin-dependent quantum device.

PACS: 73.21.La, 73.63.Kv, 73.40.Gk DOI: 10.1088/0256-307X/37/12/127301

Quantum devices composed of quantum dots have application potentials in quantum information and quantum computing. Therefore, electron transport properties through a quantum-dot system have been the focus of much research. In recent years, spintronics related to quantum dots and their applications in spin functional devices and quantum computers have aroused extensive interest among scientific researchers. Based on quantum dots, spin-dependent quantum functional devices have been proposed and verified experimentally as a required component of quantum computing.[1–3] One may foresee that quantum dot devices can be used as integrated quantum chips in the future.

Fano resonance was observed and artificially modulated in coupled quantum-dot systems.[4–10] In a triple-arm Aharonov–Bohm (AB) interferometer, the shape of the Fano resonance can be modified by tuning the energy levels of quantum dots in each arm.[11] For a hybrid triple-quantum-dot interferometer coupled with superconductor and normal leads, the oscillation behaviors of transmission coefficients and shot noise versus the AB phase exhibit an asymmetric Fano resonance structure.[12] Parity and time-reversal symmetric complex potentials on quantum transport through one parallel-coupled double-quantum-dot structure may eliminate the decoupling phenomenon, while inducing the Fano effect.[13] In our previous work, we reported the Fano effect in a coupled quantum-dot system.[14–16] We observed two new Fano resonance peaks occurring in the conductance spectra by varying the structural parameters of a parallel-coupled triple Rashba quantum-dot system.[14] By tuning the magnitude of intradot Coulomb interaction, a Fano antiresonance peak can be reversed and a transition occurs between the resonance peak and Fano antiresonance.[15] If two quantum dots are added on each side of a parallel-coupled double-quantum-dot system, then additional Breit–Wigner and Fano resonances would occur in the conductance spectra.[16]

Reliance on electron spin transport has led to many interesting physical phenomena, such as spin valve effect,[17] spin filter[18] and giant magnetoresistance effect.[19] Therefore, extensive reports have been published on experimental and theoretical studies of spin transport properties.[20–32] In the quantum dot system, spin transport is usually obtained by considering Rashba spin-orbit interaction[24–26] or a Zeeman magnetic field.[27–30] In an AB ring, a substantial spin-polarized current occurs due to the combined effect of a magnetic flux and the Rashba spin-orbit coupling interaction.[24] For a system consisting of multiple three-quantum-dot rings, 100% spin-polarized windows occur as a Zeeman magnetic field

Supported by the National Natural Science Foundation of China (Grant No. 11447132), the "Chunhui Plan" Cooperative Scientific Research Project of China (Grant No. 6101020101), and the Science and Technology Research Program of Chongqing Education Commission of China (Grant No. KJQN201801402).
*Corresponding author. Email: kongfa.chen@fzu.edu.cn; hrbhzl@126.com
© 2020 Chinese Physical Society and IOP Publishing Ltd

is introduced.[30] Moreover, electrons with different spins are scattered differently in ferromagnetic (FM) electrodes, and therefore, the transport characteristics for spin-up and spin-down electrons are significantly different.[31,32]

Herein, we design a triple-quantum-dot interferometer coupled with two FM leads, as shown in Fig. 1. A single quantum dot and "a linear double-quantum-dot molecule" are embedded in two arms of the interferometer. Charge and spin transport properties through the system are studied using the Keldysh nonequilibrium Green's function.[33,34] We analyze the formation of Fano resonance arising from the interference between the resonant process and the non-resonant process. The spin-dependent average current is manipulated by adjusting factors such as the Zeeman magnetic field, bias voltage and spin polarization parameters of FM leads.

It is assumed that the energy levels in each quantum dot are spin degenerate. The DC bias voltage $V_{\rm DC}$ is applied to the two terminals of the interferometer with time-dependent external fields $W_{\rm L}(t) = W_{\rm L}\cos(\omega t)$ and $W_{\rm R}(t) = W_{\rm R}\cos(\omega t)$. The subscripts L and R represent the left and right leads, respectively; $W_{\rm L(R)}$ and ω are the amplitude and frequency of time-dependent external field, respectively.

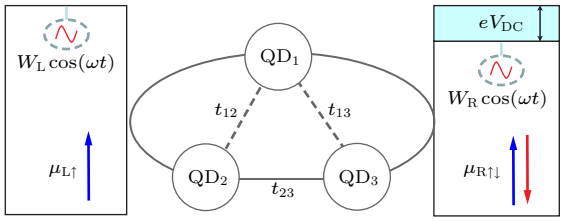

Fig. 1. Schematic diagram of a triple-quantum-dot interferometer coupled with two FM leads. A single quantum dot and "a linear double-quantum-dot molecule" are embedded in two arms of the interferometer; t_{12} and t_{13} denote the lateral coupling strengths between quantum dots in two different branches (the upper and down branches), as shown by the dashed lines. The DC bias voltage $V_{\rm DC}$ is applied to the two terminals of the interferometer with time-dependent external fields $W_{\rm L}(t) = W_{\rm L}\cos(\omega t)$ and $W_{\rm R}(t) = W_{\rm R}\cos(\omega t)$. The chemical potential of the left electrode, $\mu_{\rm L\uparrow}$, represents co-polarization and that of the right electrode, $\mu_{\rm R\uparrow\downarrow}$, denotes co-polarization or reverse polarization.

The Hamiltonian of the system can be expressed as

$$H = \sum_{\beta=L,R} H_\beta + H_{\rm dot} + H_{\rm T}. \tag{1}$$

The first Hamiltonian on the right-hand side of Eq. (1) represents the leads,

$$H_\beta = \sum_{k,\sigma} \varepsilon_{k\sigma\beta}(t) c^+_{k\beta\sigma} c_{k\beta\sigma}, \tag{2}$$

where electron energy $\varepsilon_{k\sigma\beta}(t) = \varepsilon - eW_\beta\cos(\omega t)$, $c^+_{k\beta\sigma}(c_{k\beta\sigma})$ denotes the creation (annihilation) operator of electrons in lead $\beta \in (\rm L, R)$ with a spin factor σ and the wave vector k.

The second Hamiltonian on the right-hand side of Eq. (1) describes the quantum dots

$$\begin{aligned} H_{\rm dot} = & \sum_{\sigma,j=1,2,3} (\varepsilon_{j\sigma} + \sigma B/2) d^+_{j\sigma} d_{j\sigma} \\ & - (t_{12\sigma} d^+_{1\sigma} d_{2\sigma} + t_{13\sigma} d^+_{1\sigma} d_{3\sigma} \\ & + t_{23\sigma} d^+_{2\sigma} d_{3\sigma} + {\rm H.c.}), \end{aligned} \tag{3}$$

where $\varepsilon_{j\sigma}$ is the energy level of quantum dot j, B denotes Zeeman magnetic field, $d^+_{j\sigma}(d_{j\sigma})$ represents the creation (annihilation) operator of electrons in quantum dot j, and $t_{ij\sigma}$ reflects the coupling strength between two adjacent quantum dots.

The third Hamiltonian $H_{\rm T}$ on the right-hand side of Eq. (1) describes the electron tunneling between the quantum dots and the left (right) FM leads,

$$\begin{aligned} H_{\rm T} = & \sum_{k\sigma} (t_{1{\rm L}\sigma} c^+_{k{\rm L}\sigma} d_{1\sigma} + t_{1{\rm R}\sigma} c^+_{k{\rm R}\sigma} d_{1\sigma} + t_{2{\rm L}\sigma} c^+_{k{\rm L}\sigma} d_{2\sigma} \\ & + t_{3{\rm R}\sigma} c^+_{k{\rm R}\sigma} d_{3\sigma} + {\rm H.c.}), \end{aligned} \tag{4}$$

where $t_{1\beta\sigma}$ represents the coupling strength between quantum dot 1 and the FM lead β; $t_{2{\rm L}\sigma}(t_{3{\rm R}\sigma})$ denotes the coupling strength between quantum dot 2(3) and the FM lead L(R).

Considering the wide-band approximation, the relationship between the "retarded" self-energy function and the linewidth function is as follows:

$$\Sigma^r_{\beta\sigma}(t,t') = -\frac{i}{2}\delta(t-t')\Gamma^\beta_\sigma, \tag{5}$$

where the matrix elements of Γ^β_σ read

$$\begin{aligned} \Gamma^\beta_{ll'\sigma}(\varepsilon,t,t') &= \Gamma^\beta_{ll'\sigma} \exp\left[i\int_{t'}^{t} W_\beta(\tau)d\tau\right] \\ &= 2\pi\rho_\beta t_{l\sigma\beta} t^*_{l'\sigma\beta} \exp\left[i\int_{t'}^{t} W_\beta(\tau)d\tau\right]. \end{aligned} \tag{6}$$

Here ρ_β represents the state density in the lead β. Therefore, matrix $\Gamma^{\rm L(R)}_\sigma$ can be written as

$$\Gamma^{\rm L}_\sigma = \begin{pmatrix} \Gamma^{\rm L}_{1\sigma} & \sqrt{\Gamma^{\rm L}_{1\sigma}\Gamma^{\rm L}_{2\sigma}} & 0 \\ \sqrt{\Gamma^{\rm L}_{1\sigma}\Gamma^{\rm L}_{2\sigma}} & \Gamma^{\rm L}_{2\sigma} & 0 \\ 0 & 0 & 0 \end{pmatrix} \tag{7}$$

and

$$\Gamma^{\rm R}_\sigma = \begin{pmatrix} \Gamma^{\rm R}_{1\sigma} & 0 & \sqrt{\Gamma^{\rm R}_{1\sigma}\Gamma^{\rm R}_{3\sigma}} \\ 0 & 0 & 0 \\ \sqrt{\Gamma^{\rm R}_{1\sigma}\Gamma^{\rm R}_{3\sigma}} & 0 & \Gamma^{\rm R}_{3\sigma} \end{pmatrix}, \tag{8}$$

in which the abbreviation for $\Gamma^\beta_{ll\sigma}$ is $\Gamma^\beta_{l\sigma}(l = 1,2,3)$.

The ferromagnetism on the leads is expressed by introducing a spin polarization parameter p_β for the two leads, with $p_\beta = (\Gamma^\beta_{l\uparrow} - \Gamma^\beta_{l\downarrow})/(\Gamma^\beta_{l\uparrow} + \Gamma^\beta_{l\downarrow})$, hence the linewidth matrix elements take the forms of $\Gamma^\beta_{l\uparrow(\downarrow)} = \Gamma^\beta_l(1 \pm p_\beta)$.

Using the theory of time-dependent nonequilibrium Green's function, the expression of the current can be derived,[33,34]

$$I_{\beta\sigma}(t) = -\frac{2e}{\hbar}\mathrm{Im}\int_{-\infty}^{t} dt' \int \frac{d\varepsilon}{2\pi}\mathrm{Tr}\{e^{-i\varepsilon(t'-t)}\Gamma_{\sigma}^{\beta}(\varepsilon,t,t') \cdot [G_{\sigma}^{<}(t,t') + f_{\beta}(\varepsilon)G_{\sigma}^{r}(t,t')]\}, \quad (9)$$

where $f_{\beta}(\varepsilon) = \{1+\exp[(\varepsilon-\mu_{\beta})/k_{\mathrm{B}}T]\}^{-1}$ describes the Fermi distribution function. Assume $\mu_{\mathrm{L}} = -\mu_{\mathrm{R}} = V_{\mathrm{LR}}/2$, $\mu_{\mathrm{L(R)}}$ denotes the chemical potential in the lead L(R), V_{LR} is the DC bias between the L and R leads, namely V_{DC}. According to Dyson's equation, the "retarded" Green function G^r can be obtained as follows:

$$G_{\sigma}^{r}(t,t') = \int \frac{d\varepsilon}{2\pi}\exp\Big[-i\varepsilon(t-t') - i\int_{t'}^{t} d\tau W_D\cos(\omega\tau)\Big]G_{\sigma}^{r}(\varepsilon), \quad (10)$$

where

$$G_{\sigma}^{r}(\varepsilon) = \{[g_{\sigma}^{r}(\varepsilon)]^{-1} - \Sigma_{\sigma}^{r}(\varepsilon)\}^{-1}, \quad (11)$$

in which $g_{\sigma}^{r}(\varepsilon)$ is the Fourier transform of $g_{\sigma}^{r}(t,t')$,

$$g_{jj}^{r}(t,t') = -i\theta(t-t')\exp\Big[-i\int_{t'}^{t}\varepsilon_j(t_1)dt_1\Big]. \quad (12)$$

Green's function $G^{<} = G^{r}\sum^{<}(G^{r})^{+}$, in which the "less than" self-energy function $\sum^{<}$ is

$$\Sigma^{<} = \sum_{\beta} i\int\frac{d\varepsilon}{2\pi}\exp\Big[-i\varepsilon(t-t') - i\int_{t'}^{t} d\tau W_{\beta}\cos(\omega t)\Big]f_{\beta}(\varepsilon)\Gamma^{\beta}. \quad (13)$$

The "retarded" Green's function G^r can be calculated by the equation of motion for each Green function,

$$G^{r}(\varepsilon) = \begin{pmatrix} \varepsilon-\varepsilon_1+\frac{i}{2}(\Gamma_1^{\mathrm{L}}+\Gamma_1^{\mathrm{R}}) & t_{12}+\frac{i}{2}\sqrt{\Gamma_1^{\mathrm{L}}\Gamma_2^{\mathrm{L}}} & t_{13}+\frac{i}{2}\sqrt{\Gamma_1^{\mathrm{R}}\Gamma_3^{\mathrm{R}}} \\ t_{12}+\frac{i}{2}\sqrt{\Gamma_1^{\mathrm{L}}\Gamma_2^{\mathrm{L}}} & \varepsilon-\varepsilon_2+\frac{i}{2}\Gamma_2^{\mathrm{L}} & t_{23} \\ t_{13}+\frac{i}{2}\sqrt{\Gamma_1^{\mathrm{R}}\Gamma_3^{\mathrm{R}}} & t_{23} & \varepsilon-\varepsilon_3+\frac{i}{2}\Gamma_3^{\mathrm{R}} \end{pmatrix}^{-1}. \quad (14)$$

Formulas (10) and (11) are substituted into formula (9), and the current formula is converted to

$$I_{\beta\sigma}(t) = -\frac{e}{\hbar}\int\frac{d\varepsilon}{2\pi}\mathrm{TrIm}\{2f_{\beta}(\varepsilon)\Gamma_{\sigma}^{\beta}A_{\beta\sigma}(\varepsilon,t) + i\Gamma_{\sigma}^{\beta}\sum_{\alpha=L,R}f_{\alpha}(\varepsilon)A_{\alpha\sigma}(\varepsilon,t)\Gamma_{\sigma}^{\alpha}A_{\alpha\sigma}^{+}(\varepsilon,t)\}, \quad (15)$$

where

$$A_{\beta\sigma}(\varepsilon,t) = \exp[ie(W_{\beta}-W_D)\sin(\omega t)/\omega] \cdot\sum_{\chi}\{J_{\chi}[(W_D-W_{\beta})/\omega] \cdot\exp(i\chi\omega t)G_{\sigma}^{r}(\varepsilon_{\chi})\}. \quad (16)$$

Here J_{χ} is the first Bessel function, and $\varepsilon_{\chi} = \varepsilon - \chi\omega$. The average current can be derived by calculating the time average of the current in formula (15),

$$\langle I\rangle = \frac{2e}{\hbar}\int\frac{d\varepsilon}{2\pi}\sum_{\chi}\mathrm{Tr}\Big\{\Big[J_{\chi}^{2}\Big(\frac{W_D-W_{\mathrm{L}}}{\omega}\Big)f_{\mathrm{L}}(\varepsilon) - J_{\chi}^{2}\Big(\frac{W_D-W_{\mathrm{R}}}{\omega}\Big)f_{\mathrm{R}}(\varepsilon)\Big]\Gamma_{\sigma}^{\mathrm{L}}G_{\sigma}^{r}(\varepsilon_{\chi})\Gamma_{\sigma}^{\mathrm{R}}G_{\sigma}^{\alpha}(\varepsilon_{\chi})\Big\}. \quad (17)$$

In the absence of time-dependent external field, the amplitude of time-dependent external field $W_{\mathrm{L(R,D)}} = 0$, $J_{\chi}\big(\frac{W_D-W_{\mathrm{L(R)}}}{\omega}\big) = 1$. Therefore, the average current in formula (17) can be simplified to

$$I = \frac{2e}{\hbar}\int\frac{d\varepsilon}{2\pi}\mathrm{Tr}\{[f_{\mathrm{L}}(\varepsilon)-f_{\mathrm{R}}(\varepsilon)]\Gamma_{\sigma}^{\mathrm{L}}G_{\sigma}^{r}(\varepsilon)\Gamma_{\sigma}^{\mathrm{R}}G_{\sigma}^{\alpha}(\varepsilon)\}. \quad (18)$$

At a temperature of zero, the expression of the conductance can be expressed as

$$G_e(\varepsilon) = \frac{e^2}{\hbar}\mathrm{Tr}[G^{a}(\varepsilon)\Gamma^{\mathrm{R}}G^{r}(\varepsilon)\Gamma^{\mathrm{L}}]. \quad (19)$$

Based on the above formula, we can numerically calculate the charge and spin transport characteristics through the triple-quantum-dot interferometer with or without the time-dependent external field. In the following analysis, dot-lead coupling strengths $\Gamma_1^{\mathrm{L(R)}} = \Gamma_2^{\mathrm{L}} = \Gamma_3^{\mathrm{R}} = 0.2\Gamma_0$, and Γ_0 is taken as units of energy. It is assumed that the energy levels of quantum dots $\varepsilon_1 = \varepsilon_2 = \varepsilon_3 = \varepsilon_{\mathrm{d}}$, the bias voltage between left and right leads $V_{\mathrm{DC}} = 0.05$, the temperature $T = 0.001$, the Planck constant $h = 1.0$, and the electron charge $e = 1.0$.

The influence of the interdot coupling strength $t_{12(13)}$ on the conductance is studied, as shown in Fig. 2(a). The interdot coupling can be tuned by adjusting the height and thickness of the tunneling barrier between two adjacent dots through gate voltage. According to the literature,[35,36] it is reasonable to assume that the interdot coupling strengths are the values between 0 and 3. For comparison, the conductance through the system is first studied when quantum dots 1 and 2 (3) are uncoupled (i.e., $t_{12} = t_{13} = 0$). Herein, the interferometer that we designed owns two main branches. The upper branch is left lead→dot 1→right lead, and the lower branch is left lead→dot 2→dot 3→right lead. Three conductance resonance peaks can be observed in the conductance spectra. One res-

onance peak locates at the energy level $\varepsilon = 0$ and the other two resonance peaks locate at the energy levels $\varepsilon = \pm t_{23}$. Meanwhile, an antiresonance point occurs between the energy levels $\varepsilon = -1$ and $\varepsilon = 0$. The antiresonance points are ascribed to the destructive interference of electron wave functions going through the upper and lower branches in the triple-quantum-dot interferometer. To study the specific location of the antiresonance point, the expression of conductance is given as $G_e = \frac{(0.2\Gamma_0)^2(t^2-\varepsilon^2+\varepsilon t)^2}{[(\varepsilon-t)^2+\frac{(0.2\Gamma_0)^2}{4}][(\varepsilon^2+\varepsilon t)^2+(0.2\Gamma_0)^2(\frac{3}{2}\varepsilon+t)^2]}$. It can be found from the conductance formula that two antiresonance points emerge in the conductance spectrum. One antiresonance point is at the energy levels $\varepsilon = -0.618$, and the other antiresonance point is located at the position of the energy levels $\varepsilon = 1.618$. The latter is not easily observed from Fig. 2. Because the coupling strength between quantum dot 1 and dot 2 (3) is small ($t_{12} = t_{13} < 0.1$), the variation of the three resonance peaks is very feeble. The weak coupling between quantum dots 1 and 2 (3) may be considered as a perturbation on the conductance. With the increase of $t_{12(13)}$, the energy level attraction phenomenon can be observed for the two resonance peaks located in the positive energy region. Until $t_{12(13)} \approx 0.8$, the two resonance peaks degenerate, as shown by the blue solid line in Fig. 2(b). It is worth noting that an abnormal phenomenon can be observed near the interdot coupling strength $t_{12(13)} = 1.0$ (i.e., the area surrounded by a circle of white dotted lines). To illustrate the abnormal phenomenon more clearly, Fig. 2(b) presents the curves corresponding to the conductance spectra around $t_{12(13)} = 1.0$ in Fig. 2(a). A Fano resonance can be observed clearly in the conductance spectra. The causes of Fano resonance can be analyzed as follows. It can be found that regardless of the variation of $t_{12(13)}$, a resonance peak always appears at the electron energy level $\varepsilon = t_{23}$ (except for the area surrounded by a circle of white dotted lines). An interesting phenomenon is that the position of the antiresonance point can be modulated by the interdot coupling strength $t_{12(13)}$. With increasing $t_{12(13)}$, the antiresonance point moves in the direction of the positive electron level. This shift brings the antiresonance point closer to the resonance peak at the electron energy level $\varepsilon = t_{23}$. When two states are mixed, the interference between the resonant process and the non-resonant process causes Fano resonance to be observed near $t_{12(13)} = 1.0$, as shown in Fig. 2(b). Moreover, because the antiresonance point and the resonance peak are just in contact, the resonance peak located at $\varepsilon = t_{23}$ is suppressed, leading to the decrease of the height of the resonance peak. In the meantime, an additional small resonance peak gradually emerges on the right-hand side of the antiresonance point. As the antiresonance point continues to move towards the direction of the positive electron energy level, the resonance peak located at $\varepsilon = t_{23}$ is further suppressed, thus the height of the resonance peak decreases gradually. Meanwhile, the height of the additional resonance peak on the right of the antiresonance point increases gradually. This process causes the tail direction of Fano resonance to reverse. If the antiresonance point moves out of the region of the resonance located at $\varepsilon = t_{23}$, then the degenerate energy level will return to normal. With the further increase of $t_{12(13)}$, the degenerate level splits into two resonance peaks. Therefore, three resonance peaks with a value of 1.0 appear again in the conductance spectra.

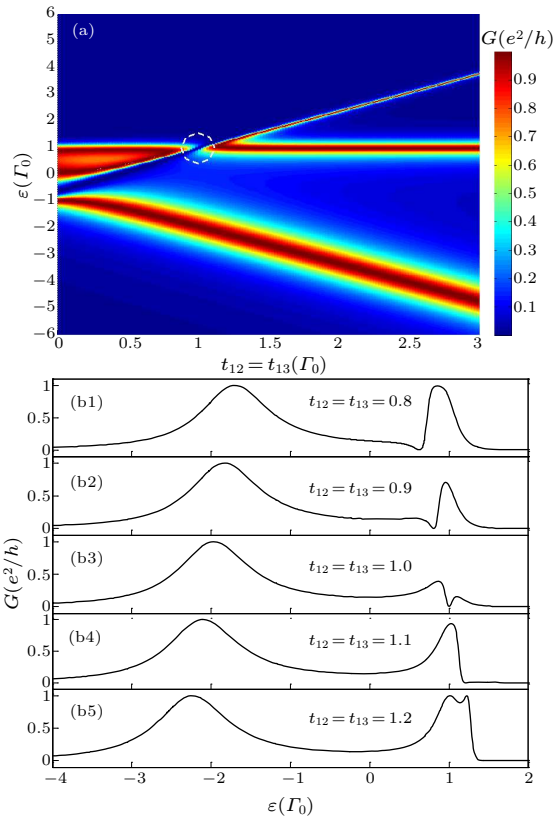

Fig. 2. (a) Contour plot of the conductance as a function of electron energy level ε and the interdot coupling strength $t_{12(13)}$; (b) conductance curves for several different values of $t_{12(13)}$ in the range of $0.8 < t_{12(13)} < 1.2$. The parameters are given by $t_{23} = 1.0$, $\varepsilon_{\rm d} = 0$, $B = 0$, $p_{\rm L} = p_{\rm R} = 0$, and $W_{\rm L} = W_{\rm R} = 0$.

Figure 3 illustrates the spin polarization $p_{\rm I} = (G_\downarrow - G_\uparrow)/(G_\downarrow + G_\uparrow)$ with respect to the electron energy level ε and $p_{\rm R}$. When $p_{\rm R}$ gradually increases from -1 to 1, the spin polarization $p_{\rm I}$ changes from -1 to $+1$ except the energy level $\varepsilon = -2.0$ and $\varepsilon = 1.0$. It can be found that the slope of the curve of spin polarization with $p_{\rm R}$ is 1.0. However, the spin polarization at the electron energy level $\varepsilon = 1.0$ exhibits abnormal behavior with a slope of -1.0. This abnormal phenomenon is mainly caused by the appearance of Fano

antiresonance. This allows us to switch the spin polarization $p_{\rm I}$ between -1 and 1 by setting the electron energy levels $\varepsilon = 1.0$ or $\varepsilon \neq 1.0$. According to this feature, the system can be designed as a spin filter. Moreover, when $p_{\rm R} = 0$, the spin-up conductance is the same as spin-down one, and therefore the spin polarization $p_{\rm I} = 0$. However, $p_{\rm I} = 1$ if $p_{\rm R} = 1$ except the location of the energy level $\varepsilon = 1.0$. Therefore, the spin polarization $p_{\rm I}$ can be converted between 0 and 1 by controlling the parameter $p_{\rm R} = 0$ or 1. Based on this property, the system can be designed as a spin-polarized pulse device.

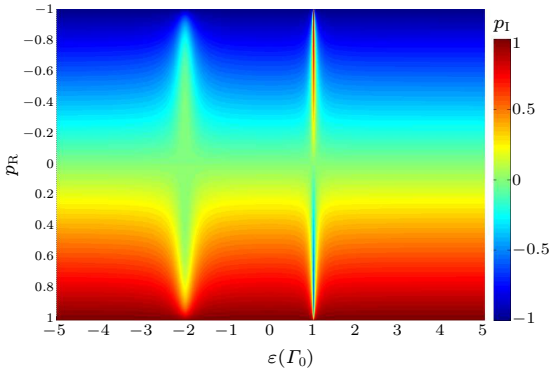

Fig. 3. Spin polarization $p_{\rm I}$ as a function of electron energy level ε and the parameter $p_{\rm R}$. The relative parameters are $t_{12} = t_{13} = t_{23} = 1.0$, $\varepsilon_{\rm d} = 0$, $B = 0$, $p_{\rm L} = 0$, and $W_{\rm L} = W_{\rm R} = 0$.

Figure 4 depicts the changes of spin polarization $p_{\rm I}$ with the electron energy level ε and $p_{\rm R}$ under the action of a Zeeman magnetic field. If a small Zeeman magnetic field B is applied ($B = 0.02$), as shown in Fig. 4(b), then the spin polarization $p_{\rm I}$ will change very little near the electron energy level $\varepsilon = -2.0$, whereas $p_{\rm I}$ changes greatly near the electron energy levels $\varepsilon = 1.0$ and $\varepsilon = 2.0$. This phenomenon is mainly due to the combined Fano effect and Zeeman effect. The abnormal phenomenon can be observed in spin polarization spectra, as denoted by the two arrows in Figs. 4(a)–4(d). The reasons for the appearance of the abnormal phenomena can be explained by the conductance formula. As $t_{12} = t_{13} = t_{23} = t$, the conductance through the system can be derived,

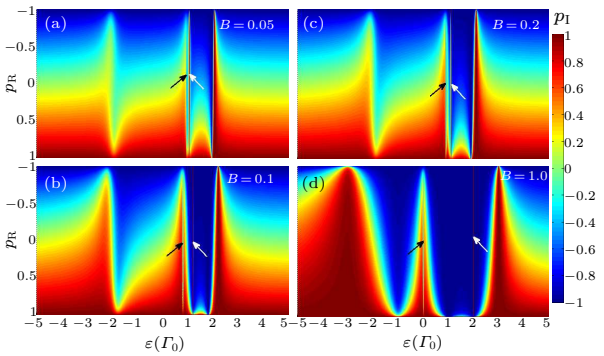

Fig. 4. Spin polarization $p_{\rm I}$ as a function of electron energy level ε and the parameter $p_{\rm R}$. The parameters are given by $t_{12} = t_{13} = t_{23} = 1.0$, $\varepsilon_{\rm d} = 0$, $p_{\rm L} = 0$, $W_{\rm L} = W_{\rm R} = 0$, and (a) $B = 0.05$; (b) $B = 0.1$; (c) $B = 0.2$; (d) $B = 1.0$.

$$G_e = \frac{(0.2\Gamma_0)^2(1+\sigma p_{\rm R})[(\varepsilon-\sigma B)^2 - 3(\varepsilon-\sigma B)t + 2t^2]^2}{[(\varepsilon-\sigma B-t)^2 + \frac{(0.2\Gamma_0)^2(1+\sigma p_{\rm R})}{4}]\{[(\varepsilon-\sigma B)^2 + (\varepsilon-\sigma B)t - 2t^2]^2 + (0.2\Gamma_0)^2(1+\sigma p_{\rm R})[\frac{3}{2}(\varepsilon-\sigma B) - t]^2\}}.$$

By analyzing the formula, it can be found that in the absence of Zeeman magnetic field (namely $B = 0$), two antiresonance points appear at the locations of the energy levels $\varepsilon = t$ and $\varepsilon = 2t$, respectively. As a Zeeman magnetic field is applied, the energy levels split. Thus, the four antiresonance points appear at $\varepsilon = t + \sigma B$ and $\varepsilon = 2t + \sigma B$, respectively. This leads to the appearance of the abnormal phenomena. The reverse polarizability is formed at $\varepsilon = t + \sigma B$, as shown by the blue line (as denoted by the black arrow) and red line (as denoted by the white arrow) in Fig. 4. The red thin line indicates a spin polarization of 100%, and the blue thin line indicates a spin polarization of -100%. The positions of the blue and the red lines shift with the change of Zeeman magnetic field intensity, as shown in Figs. 4(a)–4(d). Moreover, the two antiresonance points at the energy level $\varepsilon = 2t + \sigma B$ also affect the spin polarization. The spin polarizability located at the energy level $\varepsilon = 2t + B$ is 100%, while the spin polarizability at $\varepsilon = 2t - B$ is -100%.

Figure 5 illustrates the curves of average spin-dependent current varying with the energy level of quantum dots $\varepsilon_{\rm d}$ with or without a time-dependent external field. Here, we only study the influence of the parameter $p_{\rm R}$ on average spin-dependent current, and the Zeeman effect is not taken into consideration. In the absence of time-dependent external field, as shown by the inset in Fig. 5, a peak emerges at the energy level $\varepsilon_{\rm d} = 2.0$, and a small Fano resonance is observed at energy level $\varepsilon_{\rm d} = -1.0$. As a time-dependent external field is introduced, side-band resonance peaks occur on both sides of $\varepsilon_{\rm d} = 2.0$. The gap between adjacent resonance peaks corresponds to the photon energy of $\hbar\omega$. By applying a time-dependent external field to quantum dot system, electrons interact with the external field, exchanging discrete energy by absorbing and emitting photons, equivalently. Therefore, an electron with energy ε can be transferred to sidebands at $\varepsilon + n\hbar\omega$. This leads to the photon-assisted tunneling phenomenon, i.e., the appearance of side-

band resonance. Moreover, side-band Fano resonances can be observed on both sides of $\varepsilon_{\rm d} = -1.0$. In the positive energy level region, the spin-up current is always greater than the spin-down one. However, at $\varepsilon_{\rm d} = -1.0$ and around the energy level $\varepsilon_{\rm d} = -2.0$ in the negative energy level region, the spin-up current curve intersects with the spin-down one.

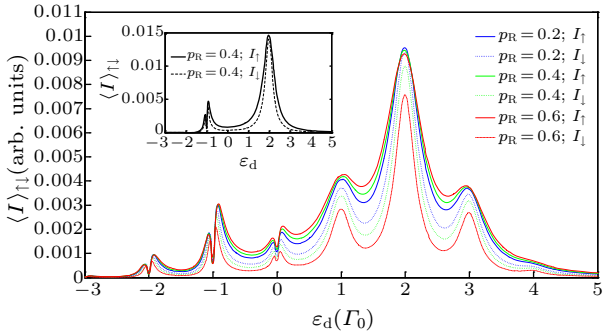

Fig. 5. Under the action of time-dependent external field, spin-dependent average current versus the energy level of quantum dots $\varepsilon_{\rm d}$. The solid and the dotted lines represent the spin-up and spin-down average currents, respectively. The blue curve denotes $p_{\rm R} = 0.2$, the Green curve denotes $p_{\rm R} = 0.4$, and the red curve denotes $p_{\rm R} = 0.6$. The relative parameters are $t_{12} = t_{13} = t_{23} = 1.0$, $\varepsilon = 0$, $B = 0$, $p_{\rm L} = 0$, $\omega = 1.0$, and $W_{\rm L} = W_{\rm R} = 1.0$.

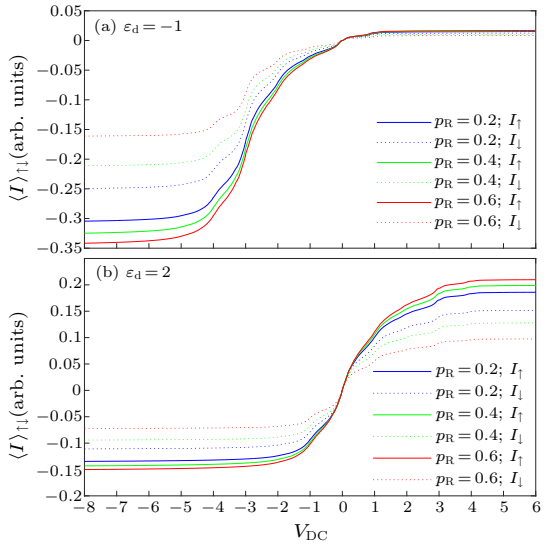

Fig. 6. Spin-dependent average current-voltage characteristics, with parameters being $t_{12} = t_{13} = t_{23} = 1.0$, $\varepsilon_{\rm d} = 0$, $B = 0$, $p_{\rm L} = 0$, $\omega = 1.0$, $W_{\rm L} = W_{\rm R} = 1.0$ and (a) $\varepsilon_{\rm d} = -1.0$; (b) $\varepsilon_{\rm d} = 2.0$.

Figure 6 presents the I–V characteristic curves for $\varepsilon_{\rm d} = -1.0$ and $\varepsilon_{\rm d} = 2.0$. From the I–V curves, it can be seen that both the spin-up and spin-down currents show multi-step phenomena, which are related to the occurrence of side-band resonances by the photon-assisted tunneling. It can be found that the magnitude of the spin polarization increases with the increase of $p_{\rm R}$. For $\varepsilon_{\rm d} = -1.0$, as illustrated in Fig. 6(a), the amplitude of spin polarization becomes larger as a relatively large negative bias voltage is applied, while the amplitude of spin polarization changes less when the positive bias voltage is applied. Moreover, the current is relatively large as the reverse bias is applied. However, the current is relatively small as the positive bias voltage is applied. If $\varepsilon_{\rm d} = 2.0$, as shown in Fig. 6(b), the spin polarization is large regardless of applying a relatively large positive bias or negative bias.

In conclusion, we have theoretically studied the conductance and average current through triple quantum dots attached to two ferromagnetic leads. The conductance and spin polarization are discussed first in the absence of a time-dependent external field. With the increase of the interdot coupling strength, an antiresonance point and the resonance peak gradually approaches, superpose, and eventually separate from each other. This leads to the interference between the resonant process and non-resonant process and thereby the occurrence of Fano effect. The spin polarization $p_{\rm I}$ can be converted between 0 and 1 by setting the parameter $p_{\rm R} = 0$ or 1. Based on this property, the system can be designed as a spin-polarized pulse device. Due to the combined Fano effect and Zeeman effect, the electron transport for spin-up electron is restrained. Meanwhile, side-band Fano resonances were observed in the presence of a time-dependent external field. Through the I–V characteristic curves, both the spin-up and spin-down currents show multi-step phenomena. The spin polarization is enhanced due to the Fano resonance. These findings provide insights into the design of a quantum device and quantum computation in the future.

References

[1] Elzerman J M, Hanson R, van Willems B L H, Witkamp B, Vandersypen L M K and Kouwenhoven L P 2004 *Nature* **430** 431

[2] Kiyama H, Nakajima T, Teraoka S, Oiwa A and Tarucha S 2015 *Phys. Rev. B* **91** 155302

[3] Kaasbjerg K and Jauho A P 2016 *Phys. Rev. Lett.* **116** 196801

[4] Zhao X, Yuan R Y, Ji A C, Yan H and Guo Y 2014 *J. Appl. Phys.* **116** 103517

[5] Zhao H K and Zou W K 2015 *Phys. Lett. A* **379** 389

[6] Ma Z S, Zhu Y, Li X Q, Lin T H and Su Z B 2004 *Phys. Rev. B* **69** 045302

[7] Gong W J, Zheng Y S, Liu Y and Lü T Q 2006 *Phys. Rev. B* **73** 245329

[8] An X T, Mu H Y, Xian L F and Liu J J 2012 *Chin. Phys. B* **21** 077201

[9] Bao X L, He Z L and Chen K F 2020 *Indian J. Phys.* (in press)

[10] Wu S Q, Wand S J, Sun W L and Yu W L 2003 *Phys. Lett. A* **307** 60

[11] Li Y X 2007 *J. Phys.: Condens. Matter* **19** 496219

[12] Zhao H K, Wang J and Wang Q 2014 *Phys. Lett. A* **378** 1553

[13] Zhang L L, Zhan G H, Li Z Z and Gong W J 2017 *Phys. Rev. A* **96** 062133

[14] He Z L, Lü T Q, Cui L, Xue H J, Li L J and Yin H T 2011

Chin. Phys. B **20** 117303
[15] He Z L, Lü T Q, Li H, Li L J, Cui L and Xue H J 2011 *Phys. Scr.* **84** 035703
[16] He Z L, Li Q, Chen K F, Bai J Y and Dang S H 2018 *Chin. Phys. Lett.* **35** 097301
[17] Ma J M, Zhao J, Zhang K C, Peng Y J and Chi F 2011 *Nanoscale Res. Lett.* **6** 256
[18] Kondo K 2016 *New J. Phys.* **18** 013002
[19] Zhang X G and Xiang T 2012 *Int. J. Quantum Chem.* **112** 28
[20] An X T, Mu H Y, Li Y X and Liu J J 2011 *Phys. Lett. A* **375** 4078
[21] Yang X, Zheng J, Chi F and Guo Y 2015 *Appl. Phys. Lett.* **106** 193107
[22] Li J L and Li Y X 2010 *Chin. Phys. Lett.* **27** 057202
[23] He Z L and Lü T Q 2012 *Phys. Lett. A* **376** 2501
[24] Sun Q F, Wang J and Guo H 2005 *Phys. Rev. B* **71** 165310
[25] Yin H T, Lü T Q, Liu X J and Xue H J 2009 *Chin. Phys. Lett.* **26** 047302
[26] Bai J Y, He Z L and Yang S B 2014 *Acta Phys. Sin.* **63** 017303 (in Chinese)
[27] Ellenberger C, Ihn T, Yannouleas C, Landman U, Ensslin K, Driscoll D and Gossard A C 2006 *Phys. Rev. Lett.* **96** 126806
[28] Fu H H and Yao K L 2012 *Appl. Phys. Lett.* **100** 013502
[29] Fu H H and Yao K L 2012 *J. Appl. Phys.* **111** 094512
[30] He Z L, Bai J Y, Ye S J, Li L and Li C X 2017 *Chin. Phys. Lett.* **34** 087301
[31] Bociana K and Rudzinski W 2013 *Eur. Phys. J. B* **86** 439
[32] Trocha P and Weymann I 2015 *Phys. Rev. B* **91** 235424
[33] Wingreen N S, Jacobsen K W and Wilkins J W 1989 *Phys. Rev. B* **40** 11834
[34] Jauho A P, Wingreen N S and Meir Y 1994 *Phys. Rev. B* **50** 5528
[35] Shangguan W Z, Au Y T C, Yu Y B and Kam C H 2001 *Phys. Rev. B* **63** 235323
[36] de Ladrón G M L and Orellana P A 2006 *Phys. Rev. B* **73** 205303